033297

3D-DEMO

Single step 3D DEposition of complex nanopatterned Multifunctional Oxides thin films

Specific targeted research project (STREP)

Priority 3: Nanotechnologies and nanosciences, knowledge-based multifunctional materials and new production processes and devices (NMP).

Publishable final activity report

Period covered: from 01/11/2007 to 30/04/2010
Date of preparation: 26/06/2010

Start date of project: 01/11/2006 Duration: 42 months

Project coordinator name: Paul Muralt
Project coordinator organization name: EPFL

Revision 1.4

Project Co-ordinator Reference

Organisation: *EPFL, LC-IMX-STI, Station 12, CH-1015 Lausanne, Switzerland*
Responsible person: *Paul Muralt*
Phone: *+41-21-6934957*
Fax: *+41-21-6935810*
E-mail: *paul.muralt@epfl.ch*

TABLE OF CONTENT

Plans and objectives

The objective of this project was to study growth and characterization of complex oxide thin films for electro-optic and piezoelectric applications. The materials in the focus were the lead-free family of alkali and earth alkali niobates, which excel in many aspects concerning piezoelectric and electrooptic properties. A central topic was the establishment of a new type of high-vacuum chemical vapor deposition (HVCVD) method that is based on a multitude of individually controllable, directed precursor beams (Chemical Beam Epitaxy, CBE) for optimizing the film uniformity on large wafers, or on the contrary, to produce compositional gradients in order to carry out combinatorial experiments. A further advantage of HVCVD is the possibility to combine chemical precursors with high energetic laser and electron beams, which allows for selective depositions, local microstructure control, or eventually local doping. Pulsed laser deposition (PLD) - a technique for small samples only - was used as complimentary or back-up method. This method permits a faster advancement in materials and characterization knowledge.

Different test structures or test devices were foreseen: Thin film wave guides (1.5 µ m), frequency doubling, and wave trapping in ring oscillators; and piezoelectric properties in bulk acoustic wave resonators. On a microscopic level, Scanning Near-field Optical Microscopy (SNOM) was employed to study optical uniformity and patterned features. The project included industrial partners for CBE hardware development (ABCD), for providing optimized CVD precursors (SAFC Hitech), and state-of-the art substrates of $LiNbO_3$ (LN) and $LiTaO_3$ (LT) (SAES GETTERS). These substrates are ideal to combine the new thin films with existing technology based on LN and LT single crystals.

Partners of the consortium and their roles:

	#	Participant Name	Short name		Scientific role
CO	1	Ecole Polytechnique Fédérale de Lausanne EPFL	EPFL, (P. Hoffmann, P. Muralt)	CH	CBE, PLD Structural, dielectric, piezoelectric characterization
CR	2	ABCD Technologies	ABCD (G. Benvenuti)	CH	CBE equipment manufacturer
CR	3	SCIPROM Technology Sàrl	SCIPROM (P. Ulrich)	CH	Management support
CR	4	SAFC HITECH Ltd	SAFC (S. Rushworth)	UK	Precursors
CR	5	SAES Getters S.p.A.	SAES (R. Giannantonio)	I	LN, LT substrates, test device evaluation
CR	6	National Inst. Lasers, plasma & radiation physics	NIL (M. Dinescu)	RO	PLD Structural characterization
CR	7	CNRS UMR 6174 (FEMTO)	CNRS (M-P. Bernal)	F	SNOM
CR	8	University of Southampton	UoS (S. Mailis)	UK	Optical measurements, device design and evaluation

Section 1 - Hardware for CBE and SNOM

Most important work item in the first project year was the establishment of a new CBE reactor. A schematic cross section through the new CBE tool is shown in fig. 1. In the new reactor, implemented improvements are: higher substrate temperature, optimized shower heads for three different gases allowing for uniform impinging fluxes for all three species on the one hand, and a flux control to obtain gradients of impinging fluxes for combinatorial research on the other hand.

The development work included analytical and Monte Carlo modeling to optimize the gas shower heads. A good agreement between the two approaches was achieved. For instance one could predict the impact of a substrate tilt on impinging flux distribution. The new reactor was designed, and manufactured according to the created CAD drawings (fig. 1). The assembled machine was delivered during the 12th project month.

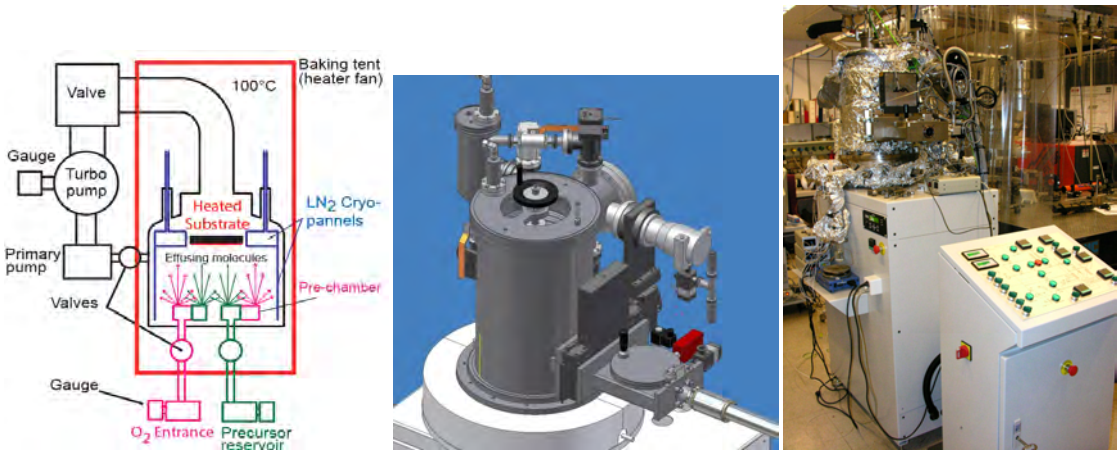

Figure 1: Schematic cross section through CBE process chamber (EPFL, left), CAD drawing of new reactor (ABCD, center), photograph of new reactor (ABCD, right).

LN and LT wafers were prepared by SAES and delivered to partners. All the wafers are double side polished and fully characterized in terms of trace elements (plasma based mass spectroscopy), crystalline quality (X-ray transmission topography), and optical absorption from 200 to 6000 nm wavelength. The first choice precursors were the metal-organic liquids of lithium tert-butoxide (Li-O-t-Bu) and niobium ethoxide ($Nb(OEt)_5$). These were synthesized and characterized by SAFC. The characterization before delivery included NMR, mass spectrometry, and thermo-gravimetric analysis to assess volatility as a function of temperature. In the following, the CBE group of EPFL and ABCD determined thermal properties of precursors (vapor pressure as a function of temperature, chemical decomposition), tested the precursor vaporization as a function of temperature, and the resulting pressure in the pre-chamber system, which governs the gas flow to the substrate.

The PLD partners NIL and the PLD group of EPFL concentrated on the following materials systems:

- $LiNbO_3$ (LN)
- Tungsten bronze $K_6Li_4Nb_{10}O_{30}$ (KLN)
- Tungsten Bronze $Sr_xBa_{5-x}Nb_{10}O_{30}$ (SBN)
- Perovskite $(K_{1/2-x}Na_{1/2-x}Li_{2x})(Nb_{1-y}Ta_y)O_3$ (KNLNT)

Most of the films were characterized with regard to structural properties, including techniques such as X-ray diffraction; secondary electron microscopy (SEM) and transmission electron microscopy (TEM), X-ray photoelectron spectroscopy (XPS), energy dispersive analysis of

X-ray emission (EDAX). At some of the films functional test were performed like the evaluation of dielectric constant, piezoelectric activity, and piezo-sensitive AFM (atomic force microscopy), and the optical index of refraction.

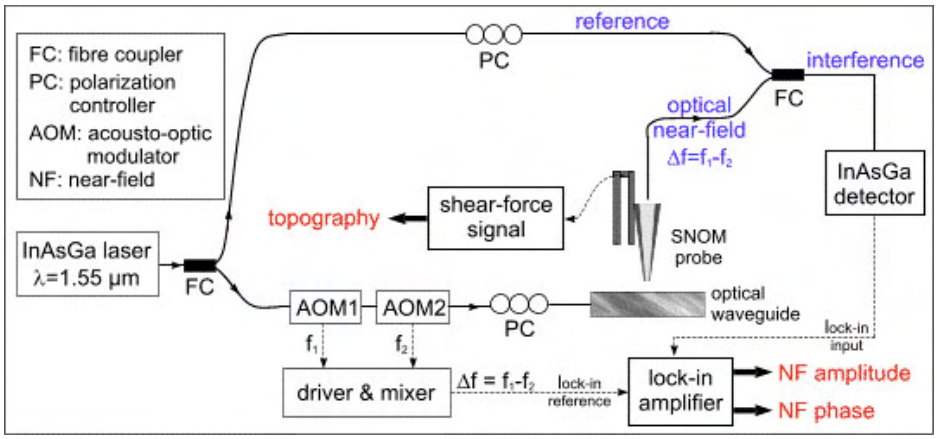

Figure 2. Schematic illustration of the heterodyne interferometer SNOM set-up.

In the first half of the project, the partners for optical characterization and devices prepared their equipment, processes, and device simulations for later applications to thin films. CNRS developed two types of optical detection methods for the Scanning Near Field Optical Microscope (SNOM). The working wavelength is 1.55 µm for both of them. The first one consists in measuring the intensity of the optical near-field. The second type of detection consists in measuring both the amplitude and the phase of the optical near-field. For this purpose, a detection based on a heterodyne interferometer has been developed within this project. The heterodyne interferometric SNOM (H-SNOM) is schematically shown on Fig. 2. Briefly, the principle of this optical heterodyne detection consists in measuring the optical intensity resulting from the interference between a reference wave and the optical near-field frequently shifted by Δf by the use of two acousto-optic modulators. The detected intensity is given by $I = A_{nf}^2 + A_r^2 + 2A_{nf}A_r\cos\left(2\pi\Delta ft + (\varphi_{nf} - \varphi_r)\right)$, where $A_{nf} = \hat{A}_{nf}\exp(i\varphi_{nf})$ and $A_r = \hat{A}_r\exp(i\varphi_r)$ are the complex amplitudes of the optical near-field and of the reference wave respectively. Taking into account that the amplitude and the phase of the reference wave keep constant during the SNOM image acquisition, the amplitude and the phase of the optical near-field is extracted by a lock-in detection at the Δf frequency. This heterodyne interferometric detection (fig. 2) is also an elegant solution to measure the very weak near-field signal collected by the SNOM probe, since it increases the signal to noise ratio.

Section 2 - Thin film results

2.1 CBE processes (EPFL)

The second project year was characterized by major achievements towards the goals of the project. The CBE tool became routinely operational up to temperatures of 750 °C, occasionally up to 850 °C. The film uniformity with all segments open was tested at various temperatures and flux intensities, using TiO_2 as model material, deposited from TTIP (Titanium Tetra-IsoPropoxide) precursor gas. Fig. 3 presents a thickness map realized by optical reflectivity measurements across a 6" wafer. From the modeling of flux distribution, a min-max uniformity of +/- 0.5 % was calculated. The measured distribution showed a very satisfying variation of +/- 2% - along one diameter even +/- 0.5 % - for a deposition at 560 °C. Possibly, temperature uniformity, tightness of gas shower head, and precision of wafer

alignment must be improved to achieve the predicted values. The showerhead was also tested for creating defined gradients in the thickness distribution of TiO_2 by selectively closing segments. The obtained gradients coincided in a satisfactory manner with the calculated impingement distributions, thus proving that the programmable shower head is useful for **combinatorial** research (fig. 3B).

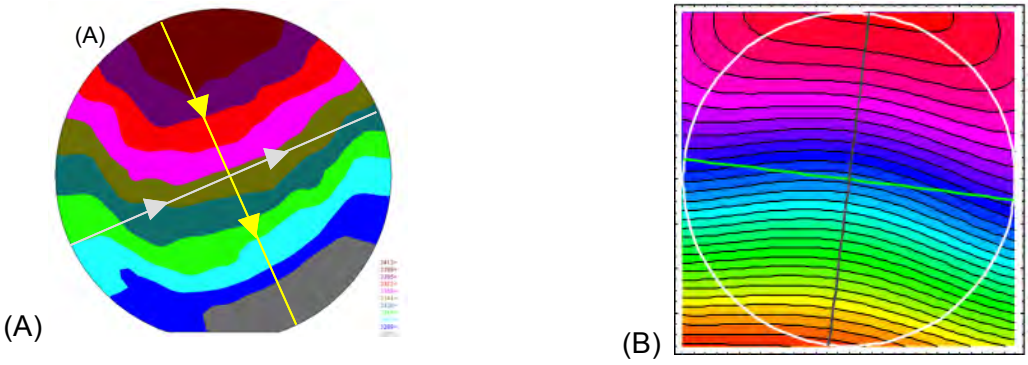

Figure 3: Optically determined thickness map of a 330 nm thick TiO2 film on a 150 mm wafer when all segments are open (A, color increment: 0.4 %), and with selectively closed segments for creating a strong thickness gradient with factor 5 variation (B, color increment: 2.6 % of maximal thickness).

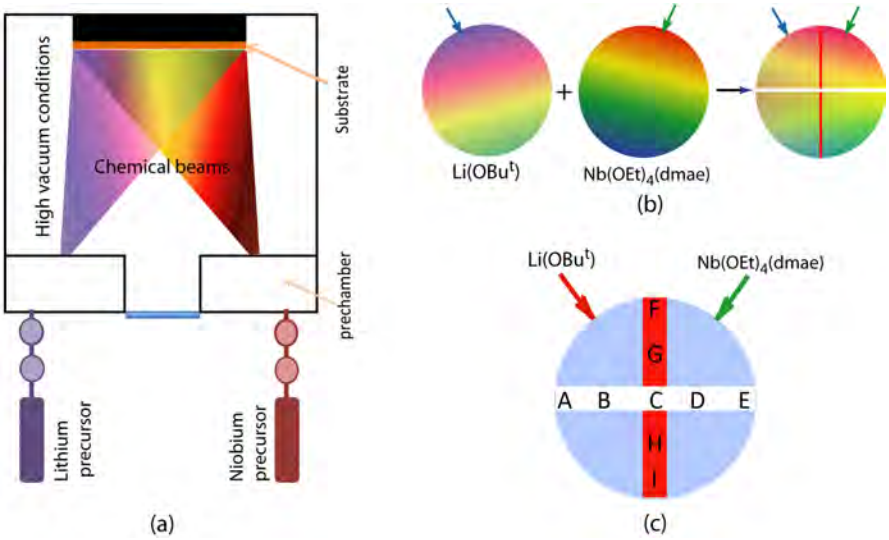

Figure 4. (a) Schematic of the chemical beam deposition machine that is able to perform combinatorial experiments. (b) Schematic of the projection of the precursor flux on the substrate and (c) positions of the sapphire slides distributed over a 150 mm diameter circular area.

Combinatorial research was used to find optimal conditions for LN film growth on (0001) sapphire substrates. SAFC developed an improved Nb precursor better suited to the deposition equipment and this proved so effective that it was adopted as the standard source for the remainder of the project. The two precursors lithium tert-butoxide (Li(OBu^t) and niobium tetra-ethoxy di-methyl-amino-ethoxide Nb(OEt)$_4$(dmae)) were supplied with two distant beams to generate a compositional gradient (left-right) and a thickness gradient (top-down) as shown in fig. 4. The best films obtained exhibit a rocking curve full-width at half-maximum of about 0.03° and a lithium content ([Li]/([Li]+[Nb])) of close to 50 mol%. Transmission electron microscopy (TEM) showed that the film grew epitaxially on sapphire with (0001) orientation and was free from large defects. An excess of lithium precursor corresponding to a Li/Nb ratio of 3.5 was giving the best result. The high-resolution TEM

images at the interface indicate the presence of an intermediate layer (see fig. 5), most likely full of dislocations to relax the stress. This can be explained by the large lattice misfit of -7.5% (RT).

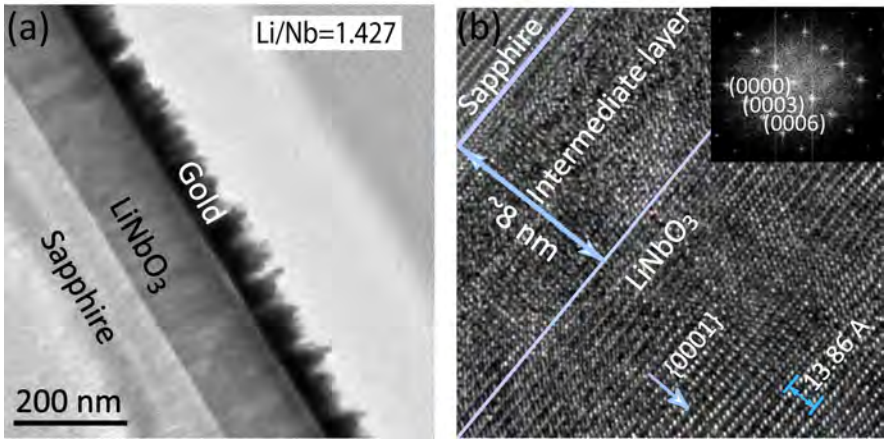

(a) (b)

Figure 5. Transmission electron microscope image of the film deposited under conditions of Li/Nb precursor ratio of 3.5. The overview of the film (a) and the high resolution image of the film at the interface (b) are depicted. The inset of (b) shows the calculated fast-Fourier transform of the epitaxial part of the film, which reveals the lattice constant of 13.86 Å along {0001} orientations.

The 170 nm thick film showed a RMS roughness of 5.5 nm. Such small surface roughness is a key to achieving low-loss optical waveguides. Raman spectroscopy proved to be a fast measurement technique for identifying the crystalline lithium niobate films close to stoichiometric composition. In future work, the thickness needs to be increased to around 400 nm in order to allow for wave guiding at 1.5 µm wavelength.

More information can be found in: A. Dabirian, S. Harada, Y. Kuzminykh, S. C. Sandu, E. Wagner, G. Benvenuti, P. Brodard, S. Rushworth, P. Muralt and P. Hoffmann, *Combinatorial chemical beam epitaxy of lithium niobate thin films on sapphire*, J.Electrochem.Soc., in press (2010).

A major challenge was the doping of LN, which intends to modify the refractive index, or to increase the maximal light intensity supported by the material. Doping with Mg has failed. However, doping with Hf was possible. Films displaying the correct crystalline phase in XRD shows considerable Hf concentrations as revealed by XPS (fig. 6). A side result of this research was the study on solid solutions of HfO_2 and Nb_2O_3. The variability of the relatively high refractive index (see fig. 7) in this system might be of interest for optical devices based on graded refractive index materials.

Published in: A. Dabirian, Y. Kuzminykh, B. Afra, S. Harada, E. Wagner, S. C. Sandu, , G.Benvenuti, S. Rushworth, P. Muralt and P. Hoffmann, *Combinatorial discovery and optimization of amorphous HfO2 – Nb2O5 mixture with improved transparency*, Electrochemical and Solid-State Letters 13**,** G60-G63 (2010).

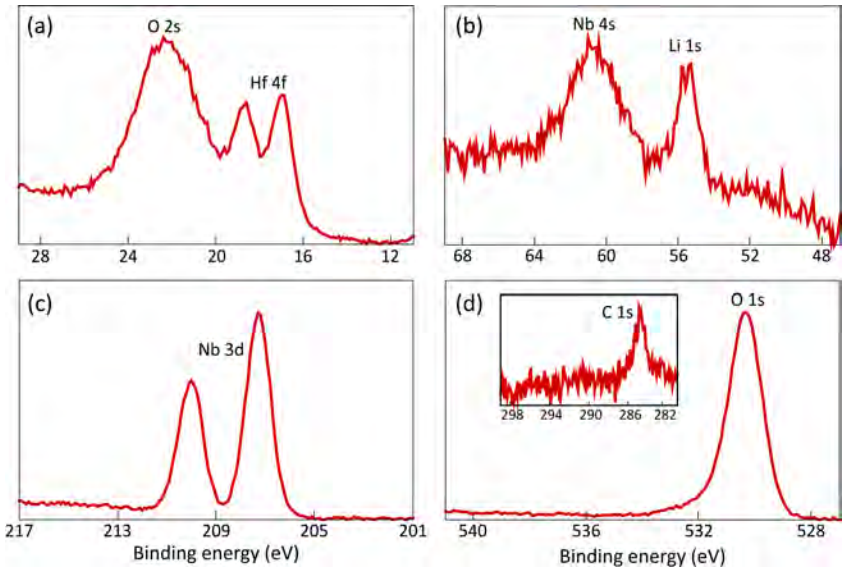

Figure 6. XPS core level spectra for the film that was produced with Hf/Nb and Li/Nb precursor ratios of 0.2 and 2.8 respectively. It confirms presence of about 6 [mol%] hafnium (Hf/(Hf+Nb)) inside the film.

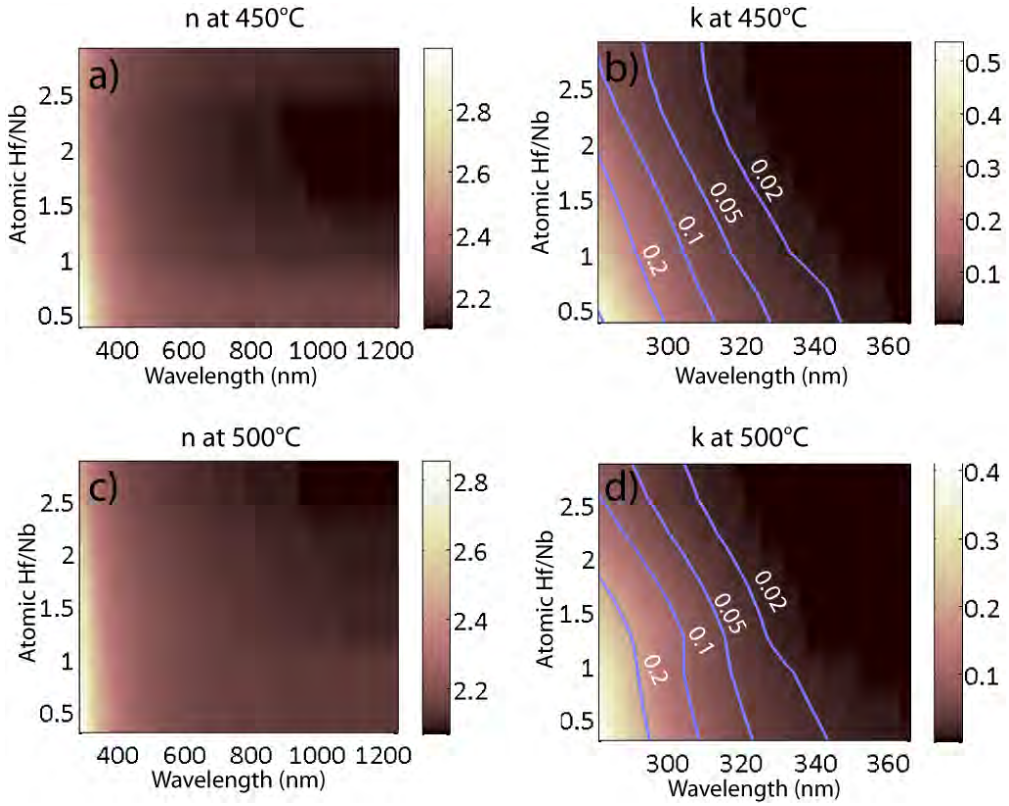

Figure 7. Spectroscopic ellipsometry measured refractive index (n) and extinction coefficient (k) for the HfO_2-Nb_2O_5 films deposited at (a, b) 450°C and (c,d) 500°C by CBE.

2.2 Pulsed Laser Deposition

2.2.1 PLD and RF-PLD of $(SrBa)Nb_2O_6$ (NIL)

Judging from single crystal properties, $(SrBa)Nb_2O_6$ (SBN) is a very interesting electro-optic material. Synthesis in thin film form is not without challenge as this material grows in the rather complex tungsten bronze structure with 10 Nb-O octahedra in the unit cell. The purpose of this study was to identify the best deposition parameters like substrate temperature, oxygen pressure, RF bias, etc., but also to find the most appropriate techniques for quantifying the electro-optic behaviour. SBN thin films were deposited by RF-PLD techniques on conductive $Nb:SrTiO_3$ (STON) single-crystal substrates of (100) orientation (see fig. 8a). The films were grown in (001) orientation. To measure largest electro-optic coefficient in SBN, which is the diagonal coefficient r_{33}, is necessary to apply an electric field along the c-axis of the film (normal to the film surface). The structural and morphological properties of SBN/STON thin films have been investigated by X-ray diffraction, atomic force microscopy and transmission electron microscopy. Different growth domains are obtained by the nature of the complex tungsten bronze whose octahedra can align in two major ways with the octahedra of the substrate. For this reason, grain boundaries are revealed by TEM images (fig 8b). For the rest, the obtained microstructure is very neat, i.e. dense and with clean interfaces.

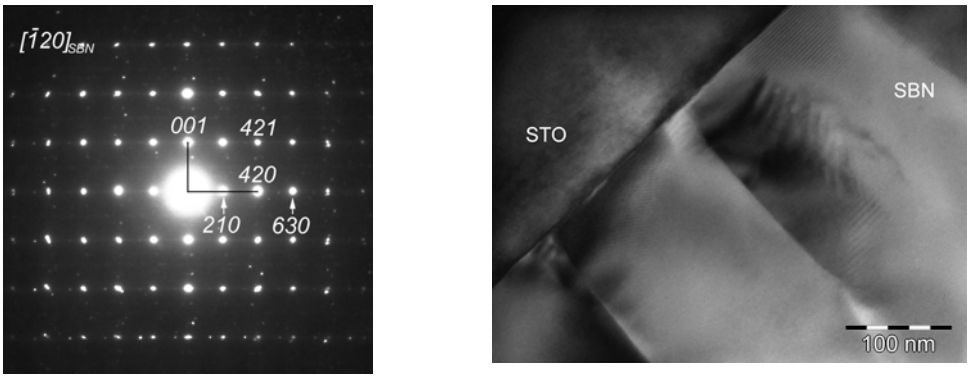

(a) **(b)**

Figure 8: (a) Electron diffraction pattern of the SBN film, all the columns have the same [1̄20] orientation, slightly rotated between them with (1-3°). (b) TEM image showing the neat STO-SBN interface.

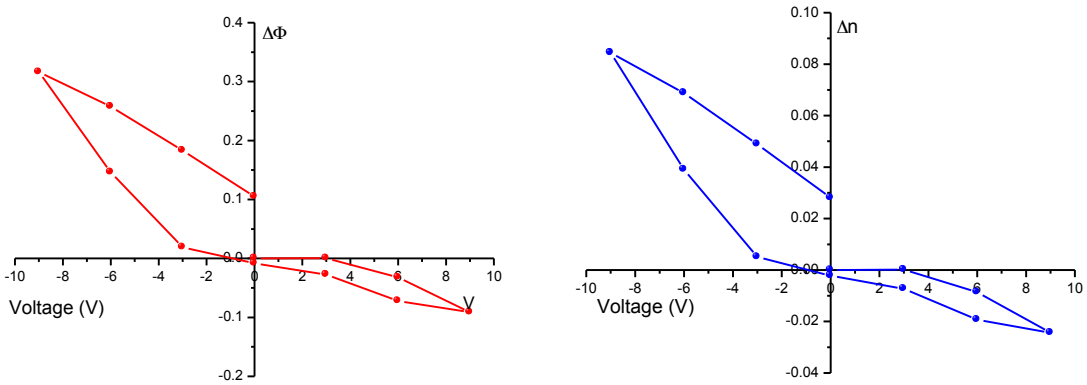

Figure 9. Electro-optic behavior for SBN:50 thin films.

Conductive transparent oxide thin films of Al doped ZnO were deposited in top of SBN/STON structures. The optical properties were evaluated by means of ellipsometry as a function of the applied DC electric field (Fig. 9). The obtained loops show that the films exhibit ferroelectric properties in as much it can be partially poled with negative voltages (top electrode). Most importantly a tunable refractive index is obtained with a Δn range of 0.12.

2.2.2 $LiNbO_3$ thin films on LT substrates by PLD (NIL)

LN films were successfully grown on LT substrates. X-ray diffraction peaks from the film could only be discriminated from the ones of the substrate by extreme grazing incidence techniques. It turned out that the films were polycrystalline. Annealing of such films was studied at UOS.

2.2.3 $LiNbO_3$ thin films on MgO substrates (EPFL)

LN and MgO have a large difference in refractive index. After the initial success of depositing (101)-oriented $LiNbO_3$ films on MgO (100) substrates in year two (and used for thin film photonic lattice, see section3), work moved towards using MgO (111) substrates. This appeared to more promising to grow (0001) oriented LN, even more as the lattice mismatch amounts to 0.2 % only. Therefore, it was expected that this substrate would be ideal for the growth of $LiNbO_3$ (001) films. Initial depositions proved to have rather high surface roughness however (see fig. 10), so attempts were made to optimise the microstructure to the levels observed when MgO (100) substrates were used. This was in response to difficulties encountered by our CNRS partners when undertaking SNOM analysis of our films. The reason for the increased surface roughness was attributed to the unstable MgO (111) surface, which is prone to both hydroxylating in air and reconstructing under the conditions necessary to deposit $LiNbO_3$. This had a subsequent effect on the epitaxial quality of any film that was deposited.

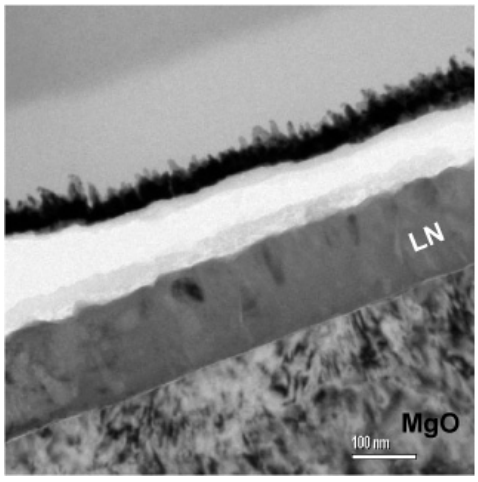

Figure 10. LN(001) thin film deposited on MgO(111) single crystal.

2.2.4 Lead free perovskite materials made by PLD (EPFL)

2.2.4.1 $(NaKLi)(NbTaSb)O_3$

Improvements were made to the microstructure of NKLNTS films deposited onto $Nb:SrTiO_3$ single-crystal substrates. These included raising the deposition temperature to 750 °C and reducing the laser pulse repetition rate from 5 Hz to 2 Hz (Fig. 11). This had the combined effect of increasing the thermal energy available to the species that made contact with the surface whilst simultaneously allowing more time for ordered, layer-by-layer growth.

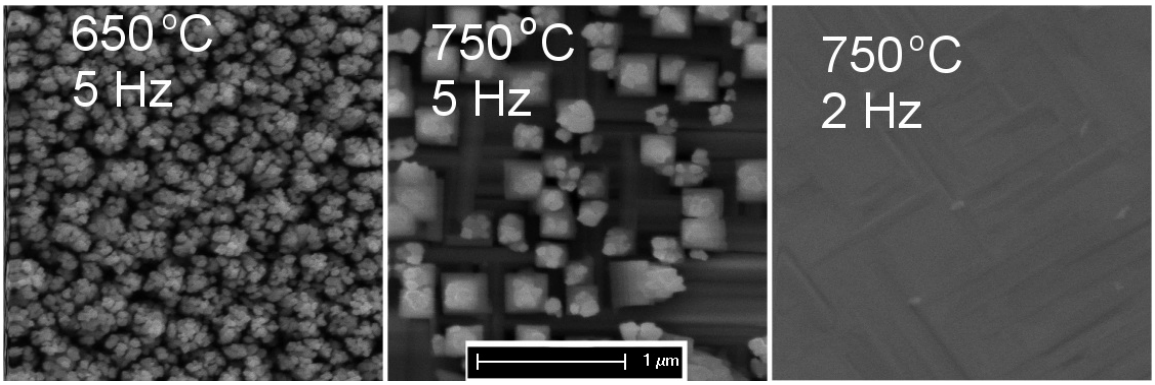

Fig. 11. SEM images showing the improvement to surface roughness of NKLNTS films on NSTO (100) substrates made possible by increasing deposition temperature and decreasing the laser repetition rate.

Dielectric measurements were made for doped and undoped NKLNTS films deposited on NSTO (100) substrates. Fig. shows the CV and loss tangent curves for NKLNTS films doped with between 0-2 mol% Mn. Doping by 1 mol% Mn had little impact on the relative permittivity, but a large effect on the loss at positive fields. The high volatility of the A-site elements leads to the formation of vacancies in the NKLNTS lattice. This in turn leads to p-type conduction and large leakage currents. It has been postulated that Mn^{2+} ions can enter the vacant A-sites, thus mitigating the p-type conduction, since they have a similar ionic radius to the ions which they replace. Since NSTO behaves as an n-type semiconductor and the undoped NKLNTS film p-type, the film-substrate interface is equivalent to a p-n junction. Under forward bias, p-n junctions exhibit conduction and this is also what is observed in the undoped film's loss curve for positive fields. Increasing the Mn-doping to 2 mol% lead to a suppression in the relative permittivity and a further reduction in loss at both positive and negative fields, when compared to undoped and 1 mol% doped films.

Polarisation hysteresis loops were also obtained for 0-2% Mn-doped NKLNTS films. Once again, the reduction in leakage current for doped films manifested itself in the observed results. Without the aid of Mn it was not possible to achieve saturation. The addition of dopants made possible the application of larger electric fields and consequently the shape of the hysteresis loops began to resemble that of a genuine ferroelectric. Piezoresponse force microscopy (PFM) was used to probe the local piezoresponse from a region of a 1 mol% Mn-doped film (Fig. 13). The predominantly bright contrast in the phase image indicates the film was out-of-plane self-polarised.

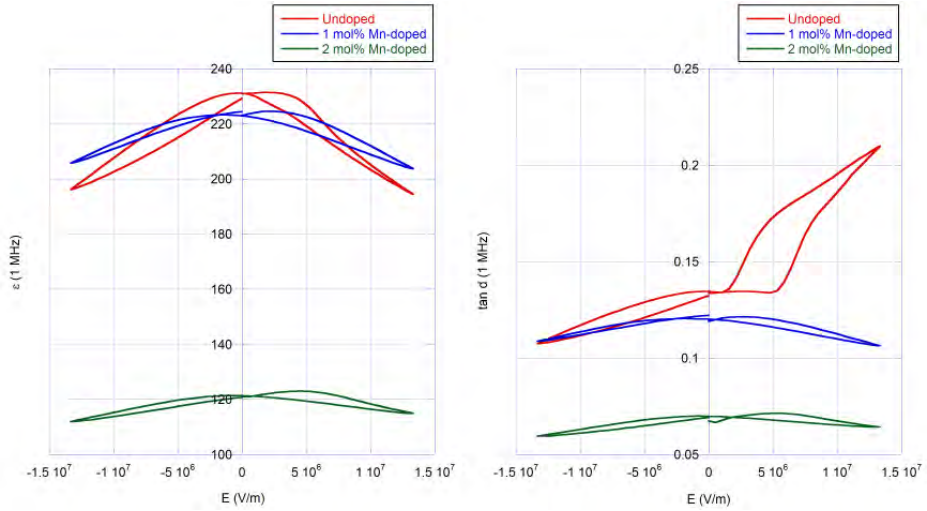

Fig. 12 CV and loss tangent curves for undoped and Mn-doped NKLNTS films.

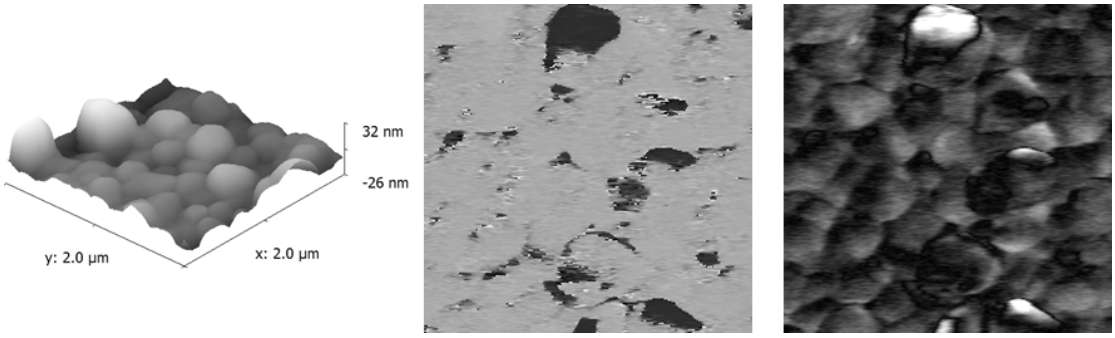

Fig. 13 Topography (left), piezoresponse phase (centre) and piezoresponse amplitude (right) associated with a 2 × 2 µm region of a 1 mol% Mn-doped NKLNTS film deposited on NSTO.

The next dopant added to the base NKLNS composition was $CaTiO_3$. Existing literature for KNN ceramics doped with $CaTiO_3$ suggested that it was beneficial in stabilising piezoelectric properties across a wider temperature range. The effect of $CaTiO_3$ doping on thin films was therefore felt worthy of investigation. The dielectric constant was found to fall with increasing $CaTiO_3$ content. Losses for both the 1.5 mol% and 3 mol% films were reduced in comparison to the undoped film; however the losses under positive fields were greater than under negative fields suggesting the presence of p-type conduction, as previously discussed. This was supported by the shape of the polarisation hysteresis loops acquired from the doped samples. It was impossible to apply a strong enough field to reach saturation, as was the case with undoped films.

Section 3 - Device Processing and Characterization

3.1 Photonic crystals obtained by Focused Ion Beam etching from bulk and thin films (CNRS)

CNRS worked on producing photonic lattices by means of focused ion beam etching, first studied at LN crystals, before applying to thin film structures. Figure 14 shows two SEM images of a hexagonal lattice of nanometric size holes etched on a titanium diffused waveguide fabricated on erbium doped lithium niobate. Hole radius is 154 nm and the period 573 nm. Form figure 3b it is quite clear that the holes are conical. Etching depth is measured to be around 1 micron.

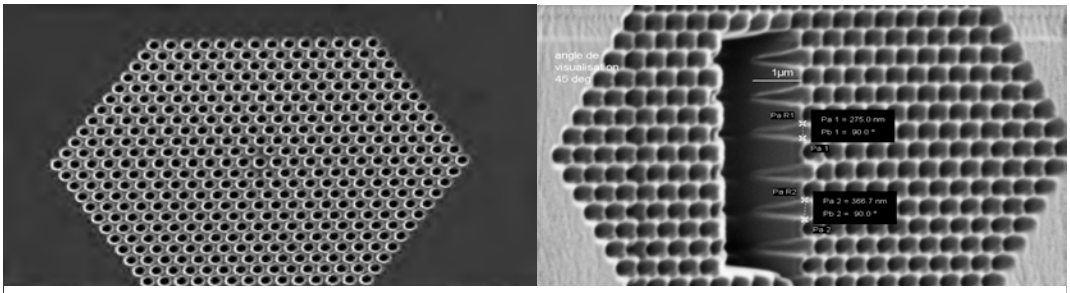

(a) (b)

Figure 14. (a) SEM image of an hexagonal lattice of air holes on erbium doped lithium niobate. (b) the conical shape of the holes can be appreciated.

A specific outcome of the project was a photonic crystal (PhC) etched into a 380 nm thick lithium niobate (LN) thin film deposited on a MgO substrate by pulsed laser deposition. The transmission properties of this novel device were assessed by optical near-field measurements, and compared to the transmission spectra of the same PhC drilled into bulk LN and calculated by a two dimensional finite-difference time domain method. We were able to show a strong improvement in the transmission properties of the LN PhC by etching the pores into a thin layer rather than into a thick LN wafer, due to the almost vertical sidewall of the holes within the film, and putting the bottom of the holes outside the wave guiding layer. This result is of great interest for the development of very efficient active devices based on LN PhCs. Moreover, the required tunable voltage will be lower in a thin film than for a bulk device.

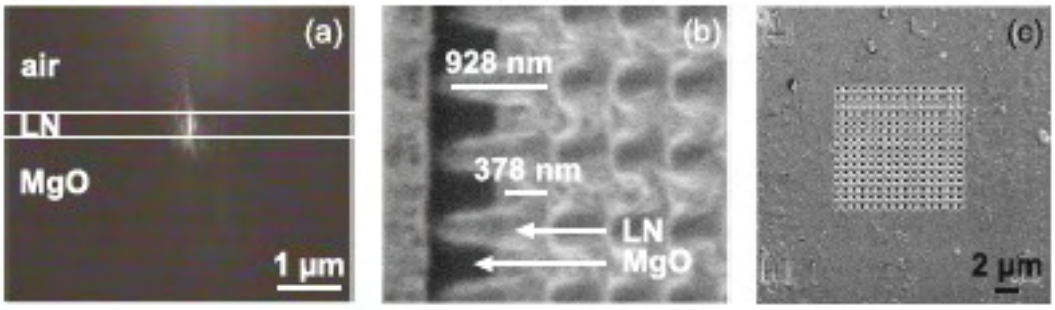

(a) (b) (c)

Figure 15. (a) Optical image of the beam leaving the edge of the substrate. (b) SEM image of the hole profiles into a LN thin film deposited on a MgO substrate by PLD. The FIB cross section exhibits the hole size and shape and the thickness of the LN layer: (c) SEM image (top view) of the photonic crystal.

Published in: S. Diziain, J.-M. Merolla, M. Spajer, G. Benvenuti, A.Dabirian, P. Hoffmann and M.-P. Bernal, Determination of local refractive index variations of thin films by heterodyne interferometric scanning near-field optical microscopy, *Review of Scientific Instruments* **80**, 093706 (2009).

3.2 3-dimensional structures by poling inhibition in $LiNbO_3$ single crystals (UoS)

3.2.1 Ridge structures

Partner UOS made simulation calculations to predict wave guiding in several types of structures, most importantly in a simple ridge structure made of LN thin film (n=2.20 @ 633 nm) on top of LT substrate (n=2.18 @ 633 nm). Beam propagation software was used to perform numerical modeling in order to evaluate the effect of the thickness of the LN film (trapezoidal shape, 6µm wide on the bottom and 4 µm wide on top) on the ability of the structure to support a waveguide mode. The thickness of the film is the most crucial fabrication parameter since the refractive indices of the film and the substrate are fixed. The cut-off height, below which no waveguide mode is supported by the structure, is the height that corresponds to an effective index equal to the refractive index of the substrate which in this case is ~2.2 µm. However, the n_{eff} is not sufficient criterion to evaluate the quality of the waveguide. It is also important to know the spatial distribution of the mode. A numerical reconstruction of the mode profile with respect to the geometrical structure is shown in figure 16. The optical power contained in mode becomes increasingly confined in the ridge superstructure with increasing height of the ridge.

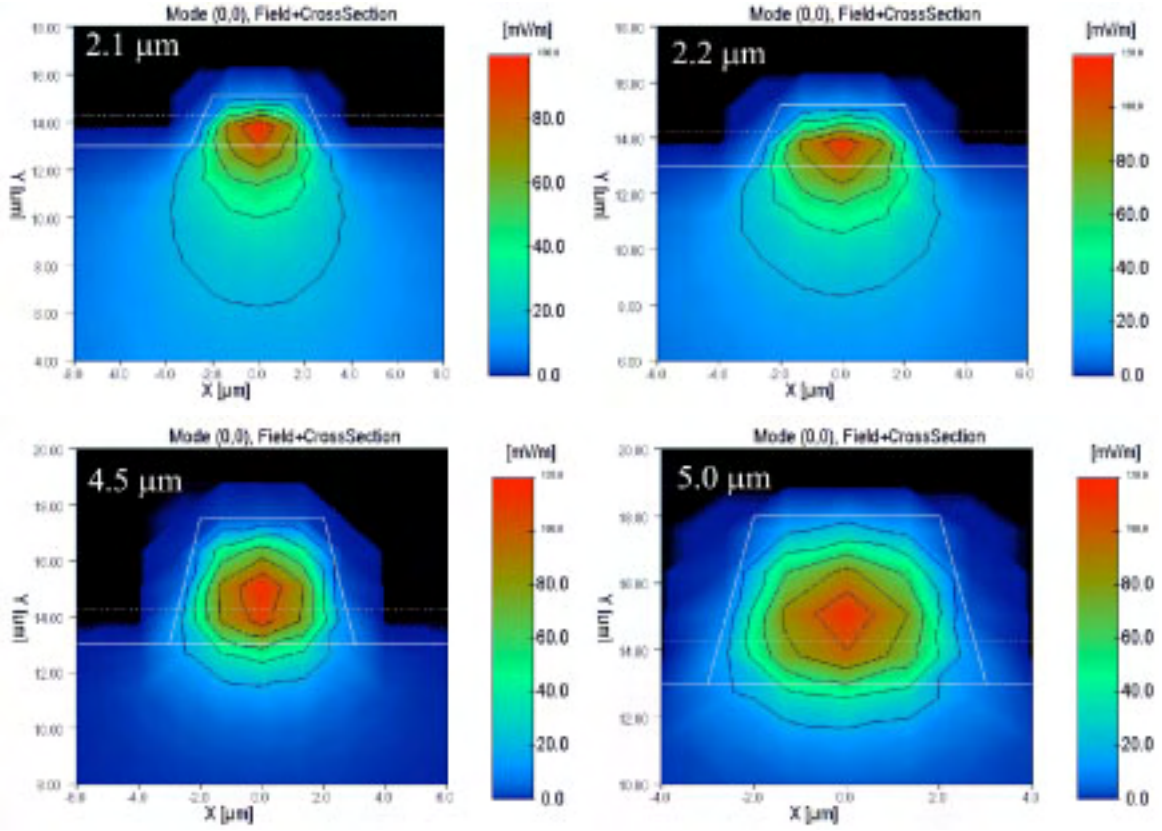

Figure 16. Profiles of the propagating waveguide modes at λ=1.55 µm for different heights of the LN ridge. Note that the vertical and horizontal scale varies between images.

Further reading: C. L. Sones, K. S. Kaur, P. Ganguly, D. P. Banks, Y. J. Ying, R. W. Eason, S. Mailis, Laser-Induced-Forward-Transfer: A rapid prototyping tool for fabrication of photonic devices, *Applied Physics A*, in press (2010). (UOS)

3.2.2 Whispering gallery mode resonators

Whispering gallery mode (WGM) resonators are photonic components, which are attracting a lot of interest as these devices can store optical power over long time intervals. They can form very narrow band optical spectral filters and if doped with laser active ions such as rare earths can form laser sources with interesting spectral characteristics. Because the resonances in such structures are very sensitive to environmental factors WGM resonators can form excellent bio-sensors. A method for the fabrication of micron-size WGM resonators in micro-structured lithium niobate has been developed within the framework of the project. The method involves domain engineering and micro-structuring of the surface of the crystal by inhibition of poling and chemical etching followed by surface tension reshaping at high temperatures, which smoothens the features (see example in fig. 17). Besides interesting geometries obtained through transformation driven by surface tension, it is also possible to tailor designed geometries such as hexagonal shapes. Resonances in a 200 μm wide hexagon could be observed.

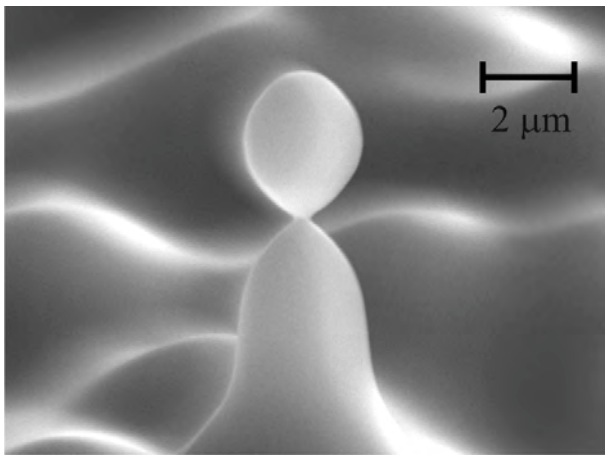

Figure 17. WGM micro-resonators produced by surface tension reshaping of domain engineered LN micro-structures

3.3 Thin film bulk acoustic wave resonators on MgO singe crystal

As to piezoelectric devices, originally we planned to fabricate a bulk acoustic wave resonator with a thin film of KNLNT. This material is based on the perovskite (K,Na)NbO_3 with additions of Li and Ta oxides (giving (K,Na, Li)(Nb,Ta)O_3) to shift the composition towards a morphotropic phase boundary with enhanced properties. It was planned to achieve a thickness mode coupling coefficient k_t^2 larger than 10 %, and a quality factor of thin film bulk acoustic wave resonators (TFBAR) of better than 500. Only PLD films were finally available for the BAW device. These films suffered from large leakage, preventing any efficient poling for large piezoelectric coefficients. As the difficult poling could also be related to the ferroelastic domains in KNLNT, which exhibits a cubic paraelectric phase, we thought to test as well a tungsten bronze structure with similar composition: KLN ($K_6Li_4Nb_{10}O_{30}$). When grown in (001) texture, the polar direction stays everywhere perpendicular to the film plane, and would be ideal for BAW applications. Although we achieved very well texture films, they turned out to be very rough. Poling did not work better than in KNLNT. We then decided to go ahead with a processing concept for BAW devices based on wet etching of MgO single crystals. To start with, we used PZT thin films.

The idea of this fabrication study was to grow epitaxial perovskite thin films on a substrate that can be wet etched to liberate free membranes of TFBAR's. It was known from the literature that MgO is such a substrate. A 100 nm thick platinum bottom electrode was deposited using a magnetron sputtering system (Nordiko 2000) at 500 °C. The bottom electrode was patterned by dry etching, using a photoresist mask, and chlorine chemistry in a dry etcher. The PZT ($Pb(Zr_{0.30}, Ti_{0.70})O_3$ in this case) was deposited onto the bottom electrode by a sol-gel process. Standard conditions were used to fabricate {100} oriented films. A $PbTiO_3$ seed layer was used to achieve high {001}-texture. A photolithographic lift-off process was used to pattern the top electrode of Pt. Another photolithography was then performed in order to define the etching holes in the PZT film. The PZT was dry etched using fluorine chemistry. The last step was the wet etching of the MgO substrate using 10 vol.% H_3PO_4 solution at 80 °C. Unfortunately we were unable to liberate the BAW membranes completely, meaning that the TFBAR lost a lot of the acoustic energy into the substrate. The admittance of the TFBAR reveals a broad resonance. The coupling coefficient k_t^2 reached a value of 23 %, however the quality factor is low due to the acoustic emission into the substrate.

All the niobate films studied so far for piezoelectric applications show large difficulties in poling. The reason is the large leakage in combination with large coercive fields. Both might be connected, in as much as defects can be responsible for increased leakage as well as for pinning ferroelectric domains. A process flow for TFBAR's on small MgO substrates was developed. However, we still have a problem in liberating the membrane completely from the substrate by surface micromachining with a wet etchant. The admittance could be measured and showed very large coupling constants in case of PZT thin films. The study shows how much more easy lead containing ferroelectrics (usually containing titanates) can be processed as compared to the alkali niobates.

Section 4 - Conclusions

A new generation of a chemical beam epitaxy (CBE) deposition tool was developed, implemented, and successfully tested for the deposition of $LiNbO_3$, and for combinatorial research. For the first time, such films were obtained by CBE. It is also for the first time that combinatorial research was demonstrated with this technique for complex, crystalline oxide thin films. In this respect, the project was very successful. One of the goals of this project was to benchmark PLD and CBE (HV-CVD) thin films. In case of LN we obtained comparable sets of data. It appears that CVD films can be deposited at lower temperatures, i.e. 500 °C rather than 700 °C. This should have an impact on cracking. Smooth PLD films on sapphire already began to crack at 500 nm thickness. It is expected that CBE films would exhibit a larger critical thickness. Unfortunately we could not show it in this project. What definitely is the case is that CBE films can be made smoother. For this reason, CBE (or HV-CVD) thin films are likely to match better the specifications for optical applications. Leakage and poling issues were problematic in all the alkali and earth alkali PLD thin films. Possibly one has to study much more dopants that could improve these materials. We could show that Mn doping lead to much lower leakage in the case of NKLNT thin films. In the case of SBN, a significant electro-optic behavior showing ferroelectric hysteresis was observed in one polarity of the electric field. The advancement in micromachining and shaping of surface structures of LN crystals shows that this approach allows a quicker progress towards real applications. Possibly one can combine such techniques with thin films (e.g. amorphous silica and metals) to realize more complex structures. The combination of single crystal LN and LT with thin films of LT and LN would be of high interest. It was found that epitaxial homoepitaxy is not trivial as the surface of the single crystal substrate becomes unstable in

the vacuum at higher temperatures. Again, CBE techniques might be more successful for such growth because of the lower deposition temperature. All the mentioned effects of roughness, cracks, leakage and poling problems are of course also detrimental for ultrasound applications in the GHz frequency range. It appears that CVD techniques might also be superior in this case. Furthermore, the project has lead to an improvement of scanning near field microscope (SNOM) techniques. The heterodyne SNOM proved to be very useful to characterize photonic structures of thin films at the nano and micron level, enabling us to demonstrate a better defined stop band edge in a thin film waveguide of LN/MgO.